In Situ Studies of Ultrasound-Stimulated Fat Crystallization Using Synchrotron Radiation

Satoru Ueno,*,† Radoljub I. Ristic,‡ Kaoru Higaki,† and Kiyotaka Sato†

Graduate School of Biosphere Sciences, Hiroshima University, 1-4-4 Kagamiyama, Higashi-Hiroshima 739-8528, Japan, and Department of Chemical & Process Engineering, University of Sheffield, Mappin Street, Sheffield S1 3JD, U.K.

Received: December 28, 2002; In Final Form: March 11, 2003

The crystallization behavior of tripalmitin (PPP) and trilaurin (LLL) without and with the application of ultrasonic power is investigated *in situ* using synchrotron radiation time-resolved small-angle X-ray scattering (SAXS) and wide-angle X-ray scattering (WAXS) simultaneous measurement. Without ultrasound application, both polymorphic forms β' and β crystallized in the melt of each substance. With ultrasound treatment of the melt, the following effects were observed: (i) a marked decrease of induction times for crystallization of both PPP and LLL, (ii) an increased nucleation rate, and (iii) a crystallization of only the β form for both PPP and LLL under conditions of initial crystallization temperatures of 50 and 30 °C, respectively, and applied ultrasound of 2 s. The last finding demonstrates that ultrasound irradiation can be used as an efficient tool for controlling the polymorphic crystallization of fats. In addition to this, the crystallization of LLL under a lower initial crystallization temperature of 25 °C and with the same ultrasonication time of 2 s, revealed the presence of both β' and β polymorphs. This suggests that the crystallization of only the β form depends not only on ultrasound treatment but also on the initial temperature of crystallization. On the basis of the dynamic nucleation of PPP and LLL crystals induced by collapsing caviatation bubbles, we argue that a pronounced decline in induction times and an increase in the nucleation rate result from the shift in the melting points due to high-pressure pulses associated with collapsing bubbles. The insufficiency of this approach in accounting for the nucleation of only the β polymorph or both β' and β polymorphs was also considered.

1. Introduction

There has been increasing interest in the application of ultrasonic waves to crystallization from different phases. In particular, this applies to the nucleation and crystallization of biological soft materials, which are often synthesized in a crystalline state. The crystallization of these materials[1] is one of the areas in which the application of ultrasonic irradiation (sonocrystallization) may play a key role, as an external factor, by controlling the crystal structure (polymorphism), shape, and rate of crystallization. The close links between these physical properties and the functional properties such as melting and solidification, dissolution, aggregation and dispersion, crystal network formation, suspension of foreign substances, and stability of crystal-containing systems increase the importance of this study.

Fats are one of the biological soft materials for which there has been a great deal of interest because of the ability to change their functional properties controllably. These materials are used in a wide range of processing industries[2−4] dealing with foods, cosmetics, pharmaceuticals, and so forth. The crystallization of fats has two major industrial uses: (i) processing of the end products made of fat crystals, such as chocolate, margarine and shortening, whipping cream, and so forth and (ii) separation of specific fat materials from natural resources such as vegetable and animal fats and oils, which contain various molecular species having different physical and chemical properties. These two processes are closely related to the polymorphic control of fats, which is usually carried out in industry by either tempering or seeding.[5] The former is applied to the chocolate or ice cream industries, whereas the latter uses certain additives such as seed crystals or templates. One of the challenges in the above processes is polymorphic control by using ultrasonication.

Considerable interest has been shown recently in the use of high-power ultrasound for encouraging nucleation and for modifying crystal growth.[6,7] It has been demonstrated that high-power ultrasound (sonication) can increase significantly the rate of nucleation in a crystallization medium.[8−10] Quite recently, sonocrystallization has been examined in confectionery fats, indicating the possibility that tempering is achieved by sonocrystallization.[11] However, the events accompanying sonocrystallization processes in fats still remain mysterious, with the need to understand them to achieve control.

We have recently studied the sonocrystallization of tripalmitin (PPP) and cocoa butter.[12] The main observations of these preliminary experiments can be summarized as follows: (a) the nucleation rate of PPP was enhanced and induction time was shortened by ultrasound application; (b) the polymorphic form V of cocoa butter was directly crystallized when ultrasound, under the optimal conditions of temperature and a period of sonication, was applied. The main disadvantage of this experiment was that one of the key measurements, X-ray analysis of the crystallizing material, was done ex situ using conventional X-ray facilities. Therefore, these results did not reflect the real-time crystallization process and were not sufficiently informative. With such results, a speculative and somewhat uncertain interpretation of the crystallization-process behavior was pos-

* Corresponding author. E-mail: sueno@hiroshima-u.ac.jp. Tel: +81-824-24-7934. Fax: +81-824-24-7910.
† Hiroshima University.
‡ University of Sheffield.

10.1021/jp027840f CCC: $25.00
Published on Web 04/29/2003

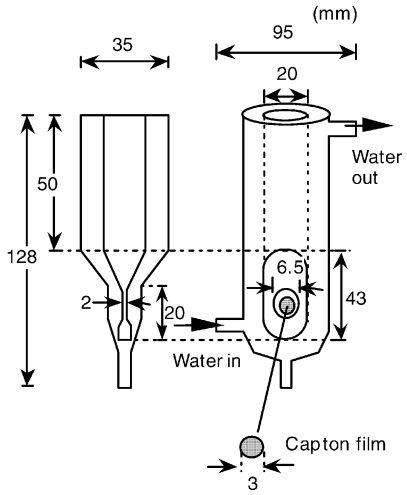

Figure 1. Handmade special-sample glass cell. The shaded circle is the window for the passage of X-ray beams through the sample. The numbers designate dimensions of the cell (in mm.).

sible. It is quite obvious that an improvement of the experimental conditions is needed.

In this paper, we treat the effects of high-power ultrasound on the crystallization behavior of typical triacylglycerols, tripalmitin (PPP), and trilaurin (LLL) examined *in situ* by time-resolved SAXS and WAXS techniques. Considering them in terms of coupling a qualitative ($T-P$) diagram for PPP and LLL and the high-pressure modified free energy for homogeneous nucleation,[13] we will test the applicability of this approach for the crystallization of triacyglycerols. More importantly, this procedure may suggest a rational way of controlling the polymorphism and nucleation rate by sonication in these industrially relevant systems.

2. Experimental Section

2.1. Materials. Tripalmitin (PPP) and trilaurin (LLL) were used as the samples and were purchased from Sigma Chemical Co. (St. Louis, MO). Both of them had a purity of more than 99% and were used without further purification.

2.2. Methods. Experiments were carried out using in situ synchrotron radiation time-resolved small-angle X-ray scattering and wide-angle X-ray scattering (SAXS/WAXS) simultaneous measurement combined with a sonocrystallization system assembled from commercial components.

Sonocrystallization was initiated with a computer-controlled ultrasound generator (model DG-100-20; Telsonic Co., Bronschhoften, Switzerland) at 20 kHz and 100 W.

The sample of 5 mL was put in a specially designed glass cell (Figure 1) jacketed by circulating water and connected to two thermostats—one for melting (hot) and the other for crystallization (cool). The window of the cell was made of a capton film of 25-μm thickness. A sample thickness exposed to synchrotron X-radiation was 3 mm. The temperature of a sample was measured by a thermocouple, with an accuracy of ± 0.5 °C. The duration of sonication was 2 s. During sonication, the sample temperature increased by approximately 2.5 °C. In both cases (without and with sonication), the sample was first melted and heated to 80 °C for PPP and 60 °C for LLL; then the sample was cooled with jacketed water to a desired level. We will call this temperature the initial crystallization temperature because once crystallization began this temperature changed because of the release of crystallization heat. The initial supercooling of melted fat, for a particular polymorph, is defined as the difference between this temperature and its melting temperature.

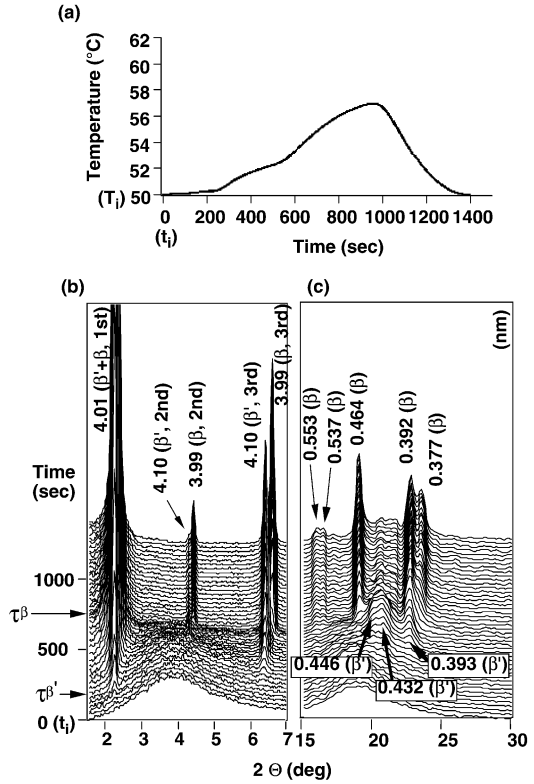

Figure 2. Experimental data for the crystallization of PPP without ultrasonication using time-resolved synchrotron radiation X-ray diffraction: (a) temperature−time evolution of the melt during crystallization, (b) SAXS, and (c) WAXS. The data were simultaneously measured.

Induction times and polymorphic forms of the crystallized samples were determined by time-resolved simultaneous SAXS/WAXS measurements. Both of these spectra must be available for an unambiguous identification of a particular polymorph because the former defines a lamellar structure with long spacing values and the latter defines a corresponding short interplanar distance of a subcell.[14] SAXS was used for induction time measurements rather than WAXS because of its higher detecting system sensitivity. Spectra were taken at 10 s intervals. However, for clarity of presentation, all spectra are not reproduced in the Figures.

Experiments presented in this work were performed at SAXS/WAXS station 8.2 at the SRS Daresbury Laboratory (U.K.). This beamline has been described extensively elsewhere.[15] SAXS/WAXS data were detected by a position-sensitive proportional counter (PSPC). The camera lengths of SAXS were 1.5 and 3.5 m for PPP and LLL, respectively. For WAXS, this length was 0.3 m for both samples. The system was operating at a wavelength of 0.154 nm.

3. Results

3.1. Crystallization of PPP without Ultrasound. Figure 2a shows the temperature−time evolution of the melt during the crystallization of PPP. The zero time, $t_i = 0$, was defined as the moment at which the melt achieved the selected initial crystallization temperature, $T_i = 50$ °C. The degree of metastability of the melt, with respect to the melting points of β' and β, was defined in terms of an absolute value of supercooling. This can be expressed for the β' form as $\Delta T_i^{\beta'} = T_m^{\beta'} - T_i$ and for β as $\Delta T_i^{\beta} = T_m^{\beta} - T_i$, where $T_m^{\beta'}$ and T_m^{β} are the melting temperatures of β' and β, respectively, whereas $T_i = 50$ °C is the initial crystallization temperature. The experimental values

TABLE 1: Melting Point (T_m, °C), Enthalpy of Fusion (ΔH, kcal/mol), and Molar Volume Change (ΔV, m^3/mol) of the β' and β Forms of PPP and LLL

	tripalmitin (PPP)		trilaurin (LLL)	
polymorph	β' form	β form	β' form	β form
T_m (°C)	56.6	66.4	35.0	46.5
ΔH (kcal/mol)	31.4	41.0	19.4	29.5
molar volume change $\Delta V \times 10^{-6}$ (m^3/mol)	150.5	167.3	106.3	123.1

TABLE 2: Initial Temperature for Crystallization (T_i, °C), Corresponding Supercooling (ΔT_i, °C), and Induction Time (τ, s) of Crystallization of the β' and β Forms of PPP and LLL without and with Ultrasound Stimulation

tripalmitin (PPP)

		polymorph	β' form	β form
$T_i = 50$ °C		ΔT_i	6.6	16.4
	τ	us = 0 s	180	760
		us = 2 s		20

trilaurin (LLL)

		polymorph	β' form	β form
$T_i = 30$ °C		ΔT_i	5.0	16.4
	τ	us = 0 s	1820	2820
		us = 2 s		30
$T_i = 25$ °C		ΔT_i	10.0	21.5
	τ	us = 0 s	60	300
		us = 2 s	40	100

of melting temperatures are given in Table 1, and corresponding initial supercoolings for both forms are given in Table 2.

Figure 2b and c shows the time-resolved SAXS and WAXS data, respectively, from the PPP crystals nucleated and grown under the temperature−time conditions described above. Identifying the diffraction peaks of these spectra confirmed that both the β' and β forms were crystallizing. The induction time of each polymorph was assessed as the time elapsed from the moment the initial crystallization temperature $T_i = 50$ °C was established until the moment at which the first appearance of an appreciable peak of a particular polymorph was detected in the SAXS spectrum. The less stable form, β', crystallized first. The induction time, which corresponds to the crystallization of this phase, is designated by $\tau^{\beta'}$ on the time scale of the SAXS spectrum. In a similar way, the induction time for the crystallization of the β form, τ^{β}, was determined. In this case, the diffraction peak of the third order of SAXS was used because of complete overlapping of the first-order peaks of β' and β. For this reason, the assessment of τ^{β} is less accurate than would be expected in the case of using the first-order diffraction peak. The assessed values of the induction times for both polymorphs are given in Table 2. This Table shows that the induction time for the β' form is significantly shorter than that for β. This is in good agreement with the Ostwald rules of stages because the β' form is less stable than the β form.

It should be noted that when the crystallization began $\tau^{\beta'} \approx$ 180 s and the temperature of the melt was still at its constant initial value ($T_i = 50$ °C) (Figure 2a). This can be explained by two facts: (a) at the beginning of the process, only β' crystallized and (b) this polymorph has a lower enthalpy of crystallization than the β form (Table 1). At the later stage of crystallization, when the β form started crystallizing simultaneously with β', a considerably larger amount of crystallizing heat was released in the bulk of the melt. This resulted in an increase in the temperature. After the maximum was achieved, the point at which a massive crystallization of the two polymorphs was completed, the temperature of the melt decreased back to its original value.

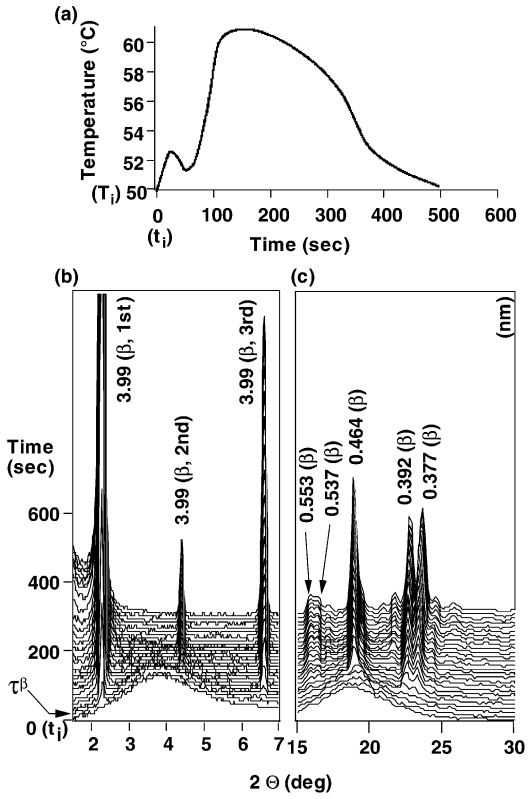

Figure 3. Experimental data for the crystallization of PPP with ultrasonication using time-resolved synchrotron radiation X-ray diffraction: (a) temperature−time evolution of the melt during crystallization, (b) SAXS, and (c) WAXS. The data were simultaneously measured.

3.2. Crystallization of PPP with Ultrasound. Figure 3a shows the temperature−time evolution of the PPP melt during its crystallization. The initial experimental conditions of the melt were almost the same as those described in the previous section. The only difference was in imposing an additional condition of sonication for 2 s, when the melt reached the same initial temperature $T_i = 50$ °C at $t_i = 0$. This led to an increase in the temperature of the melt of approximately 2.5 °C. The temperature then decreased until crystallization occurred. As we shall see later, the beginning of crystallization was defined by the induction time, $\tau^{\beta} = 20$ s, determined from the SAXS data (Figure 3b). This time corresponds to a crystallization temperature of 52.3 °C, which is slightly higher than the initial temperature of the melt. This difference was caused by the conversion of ultrasound energy to heat. From this point, the temperature continued to decrease regardless of the fact that a certain amount of heat was released in the crystallization process. This continued temperature decrease shows that the cooling, produced by the flow of jacketed water around the melt, was larger than the heating produced by the initial crystallization. This trend lasted approximately 30 s, after which time the temperature began to rise quite rapidly, achieving its second maximum and then finally decreasing to its initial value. The rise in temperature corresponds to a massive nucleation of PPP.

Figure 3b and c represents the time-resolved SAXS and WAXS spectra obtained for the crystallization process observed under the above conditions. The analysis of these two X-ray diffractograms confirms that the β form was the only crystallizing phase. This does not exclude some traces of β', which

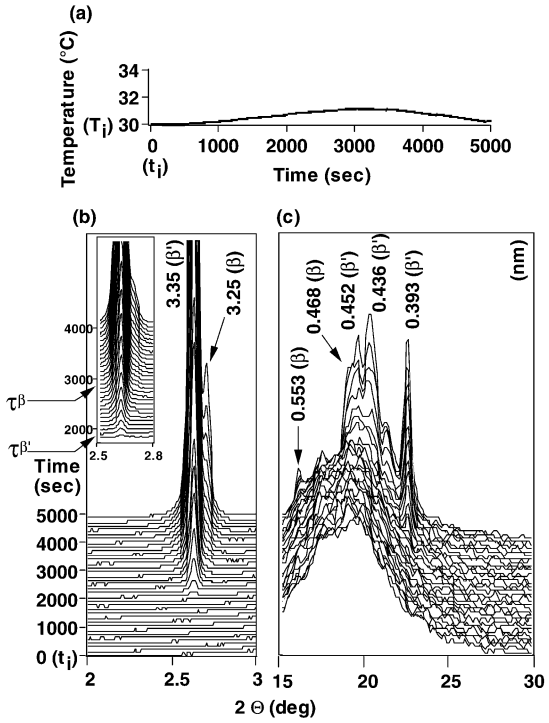

Figure 4. Experimental data for the crystallization of LLL without ultrasonication at $T_i = 30$ °C using time-resolved synchrotron radiation X-ray diffraction: (a) temperature−time evolution of the melt during crystallization, (b) SAXS, and (c) WAXS. The data were simultaneously measured.

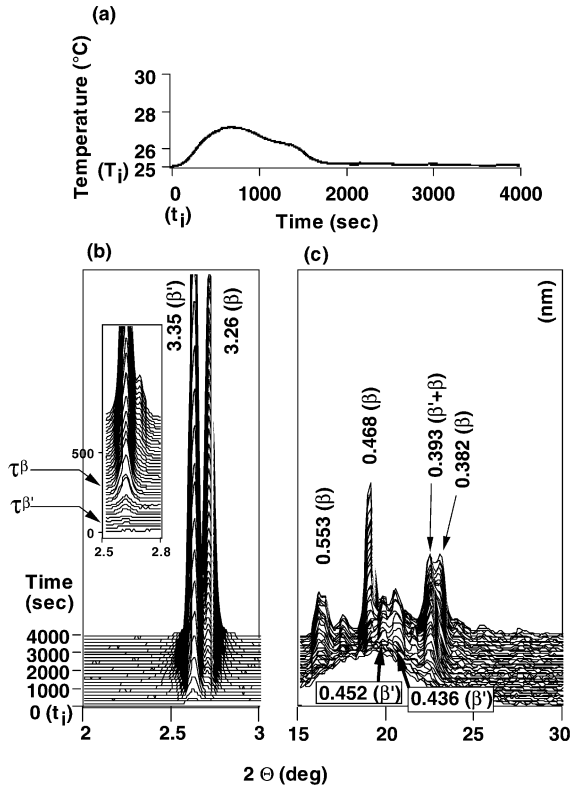

Figure 5. Experimental data for the crystallization of LLL without ultrasonication at $T_i = 25$ °C using time-resolved synchrotron radiation X-ray diffraction: (a) temperature−time evolution of the melt during crystallization, (b) SAXS, and (c) WAXS. The data were simultaneously measured.

might have crystallized, but if it does, the amount must be so small that the existing WAXS detecting system could not record it.

Because sonication was applied at $t_i = 0$, when the initial temperature $T_i = 50$ °C was achieved, the same definition of induction time as that given in section 3.1 is used. The time-resolved SAXS spectra (Figure 3b) showed that this time was approximately 20 s. This value and the experimental conditions under which the experiment was performed are given in Table 2. A comparison of this induction time with that obtained without sonication shows that sonication reduces the induction time by a factor of up to 38.

3.3. Crystallization of LLL without Ultrasound. 3.3.1. Initial Crystallization Temperature $T_i = 30$ °C. Figure 4a describes the temperature−time evolution of the LLL melt during crystallization at the initial temperature of the melt $T_i = 30$ °C. This temperature produced a supercooling for β' that was quite similar to that for β' of PPP and almost the same supercooling for β as that for β of PPP (Table 2).

Figure 4b and c show the time-resolved SAXS/WAXS spectra for the crystallization conditions indicated in Figure 4a. These spectra show clearly that both polymorphs, β' and β, were crystallized—first β' as a less stable form and then β as a stable form. The corresponding induction times $\tau^{\beta'} = 1820$ s and $\tau^{\beta} = 2820$ s were determined from the SAXS spectrum (Figure 4b) and are given in Table 2.

Because the chosen initial supercooling values for the crystallization of β' and β of the PPP melt are very similar to those of the LLL melt, it is interesting to compare the temperature−time dependencies of these two melts (Figures 2a and 4a). Unlike the temperature−time characteristics of Figure 2a, a slight temperature increase characterizes the temperature−time dependence of the LLL melt. Comparing the WAXS data for PPP with those for LLL (Figures 2c and 4c), it can be concluded that in the former case the β form dominates whereas in the latter case β' dominates. Having taken this and the corresponding values of the enthalpies of crystallization for the β form of PPP (41.0 kcal/mol) and for the β' form of LLL (19.4 kcal/mol) (Table 1) into account, the heat released during the crystallization of PPP was considerably larger than that of LLL. As a consequence, the steepness of the temperature profile, observed during the crystallization of PPP, is much larger than that observed during the crystallization of LLL.

3.3.2. Initial Crystallization Temperature $T_i = 25$ °C. The main intention of this experiment was to investigate how an increase in initial supercooling can influence the crystallization of the two polymorphic forms of LLL. For that purpose, the absolute values of the initial supercoolings, used in the previous experiment, were increased by 5 °C (Table 2). This was done by cooling the melt to $T_i = 25$ °C. The temperature−time profile of the melt during crystallization, for these initial conditions, is shown in Figure 5a.

The time-resolved SAXS and WAXS spectra, taken simultaneously with the Figure 5a data, are given in Figure 5b and c, respectively. The data show that, similar to the situation in the previous experiment ($T_i = 30$ °C), both the β' and β forms were crystallizing simultaneously, although in the initial period of crystallization up to 60 s only β' was crystallizing as a less stable form. The induction times for both forms were determined from SAXS (Figure 5b) and are given in Table 2.

Comparing the results at the two different temperatures, it can be seen that (a) the β' and β forms were crystallizing in both cases and (b) with increased supercooling the induction times for both polymorphs were significantly shorter, by 2 orders of magnitude for β' and by 1 order magnitude for β. In addition to that, a marked increase in the gradient of the temperature

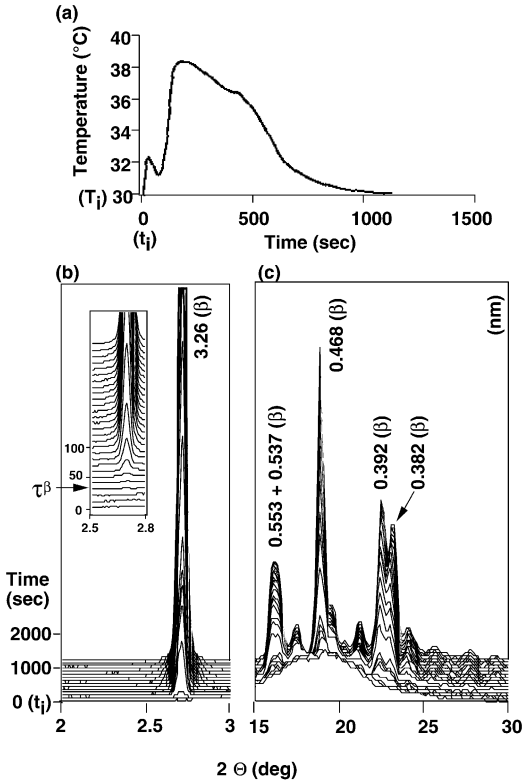

Figure 6. Experimental data for the crystallization of LLL with ultrasonication at $T_i = 30$ °C using time-resolved synchrotron radiation X-ray diffraction: (a) temperature- time evolution of the melt during crystallization, (b) SAXS, and (c) WAXS. The data were simultaneously measured.

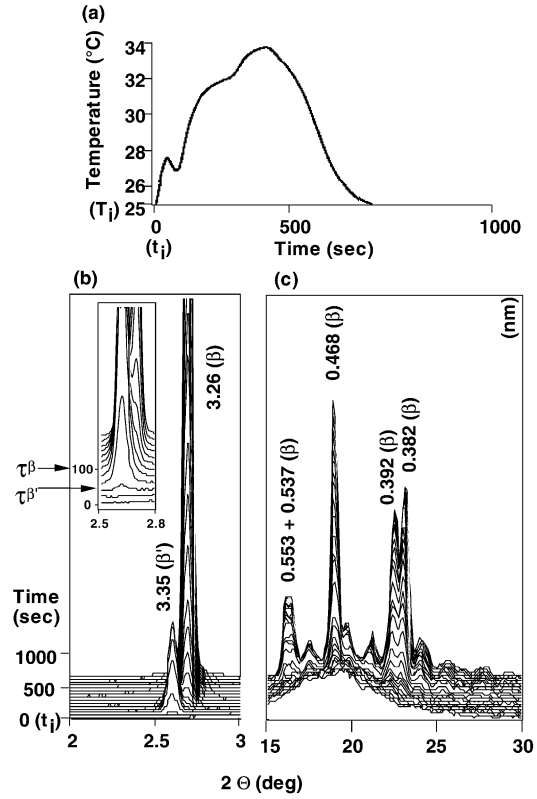

Figure 7. Experimental data for the crystallization of LLL with ultrasonication at $T_i = 25$ °C using time-resolved synchrotron radiation X-ray diffraction: (a) temperature−time evolution of the melt during crystallization, (b) SAXS, and (c) WAXS. The data were simultaneously measured.

profile was observed with larger supercoolings. This is likely to be caused by an increased number of nucleation sites of both forms.

3.4. Crystallization of LLL with Ultrasound. 3.4.1. Initial Crystallization Temperature $T_i = 30$ °C. Figure 6a shows the temperature−time profile of the LLL melt, which was sonicated at $T_i = 30$ °C. This profile shows almost the same patterns as that presented in Figure 3a. A detailed description of these patterns and their origin has already been given in section 3.2.

The analysis of the time-resolved SAXS and WAXS data, shown in Figure 6b and c, respectively, confirmed clearly that only the β form was crystallizing. This was a major finding of this experiment. The induction time for the crystallization of this polymorph was found from the SAXS spectrum (Figure 6b) and is presented in Table 2.

3.4.2. Initial Crystallization Temperature $T_i = 25$ °C. Figure 7a represents the temperature−time dependence for the crystallization of the sonicated LLL at $T_i = 25$ °C. This dependence shows a very close similarity to those presented in Figures 3a and 6a. To some extent, this similarity in the shape reflects two effects of sonication that seem to be independent of the material and initial supercooling: (1) absorption of heat and (2) stimulation of the nucleation process. The former effect is manifested by a sharp increase in the temperature just after sonication, whereas the latter one is manifested by the second pronounced temperature increase, caused by the enhanced crystallization heat released from the stimulated crystallization process.

Figure 7b and c shows the time-resolved SAXS and WAXS spectra of the crystallizing material from the sonicated melt whose initial metastability was defined by $T_i = 25$ °C. An identification of the diffraction peaks in both spectra shows that both the β' and β polymorphs were crystallized after the application of ultrasound. The induction times for these two forms were determined from the SAXS spectrum (Figure 7b) and are presented in Table 2.

The findings that only β was crystallizing from the sonicated melt at $T_i = 30$ °C and β' and β were crystallizing at $T_i = 25$ °C suggest that supercooling plays an important role in the crystallization of a particular polymorph. To obtain only the β polymorph, the most optimal conditions of sonication and supercooling of the melt are needed.

4. Discussion

To discuss our results according to the earlier proposed scenario (section 1), we need to know the temperature−pressure ($T-P$) phase diagram for each polymorph of PPP and LLL. Because these diagrams are not available at present, we will define them qualitatively by using the Clapeyron equation and the relevant experimental data concerning these two materials.

4.1. Qualitative ($T-P$) Diagram of LLL and PPP. The well-known Clapeyron equation applied to equilibrium between any two phases describing the melting process can be written as

$$\left(\frac{dT}{dP}\right)_{equil} = T\frac{\Delta V}{\Delta H} \quad (1)$$

where $(dT/dR)_{equil}$ describes the change in the melting temperature T with pressure P; ΔV is the corresponding molar volume change due to melting, and ΔH is the enthalpy of melting. For most substances including fats, $(dT/dP)_{equil}$ is positive. In addition to that, we assume that this derivative is constant for

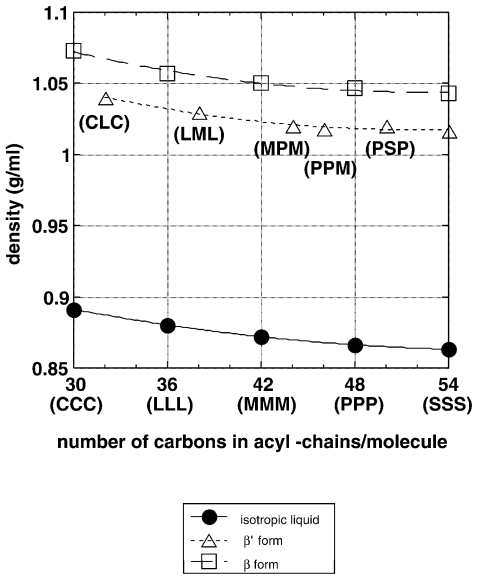

Figure 8. Relationship between the density of a fat and the number of carbon atoms present in the acyl chains of its molecule. Solid and broken lines are the least-squares fitting curves for each state of the fats. The densities were obtained from refs 16−19.

all of the polymorphs over a wide range of the ($T-P$) phase diagram. The thermodynamic properties characterizing the right side of eq 1 are experimentally known and are given in Table 1 for both PPP and LLL materials, corresponding to the β and β' forms. The exception was ΔV, which can be calculated as $\Delta V = M(\rho_s - \rho_l/\rho_s\rho_l)$, where M is molar mass, ρ_s is the density of a solid phase, and ρ_l is the density of an isotropic liquid phase (melt).

The density of any phase of a fat was determined from a corresponding dependence describing the change in the density of that particular phase as a function of the number of carbon atoms present in acyl-chain molecules of different fats (Figure 8). The three such dependencies for β, β', and an isotropic melt, shown in this Figure, were obtained by applying a least-squares fitting procedure to the available experimental data.[16−19] The data presented in this way enabled the determination of nonavailable densities of β' forms for PPP and LLL. From Figure 8, it was found that for PPP $\rho_s^{\beta'} = 1.02$ g/cm^3, $\rho_s^{\beta} = 1.04$ g/cm^3, and $\rho_l = 0.87$ g/cm^3; for LLL, $\rho_s^{\beta'} = 1.03$ g/cm^3, $\rho_s^{\beta} = 1.06$ g/cm^3, and $\rho_l = 0.88$ g/cm^3.

To predict qualitatively a ($T-P$) phase diagram for both β and β', we write eq 1 for each polymorph in its explicit form and find the ratio

$$\frac{\left(\frac{dT}{dP}\right)_{equil}^{\beta'}}{\left(\frac{dT}{dP}\right)_{equil}^{\beta}} = \frac{\frac{T_m^{\beta'}(\Delta V)^{\beta'}}{(\Delta H)^{\beta'}}}{\frac{T_m(\Delta V)^{\beta}}{(\Delta H)^{\beta}}} = \frac{\frac{T_m^{\beta'}(\rho_s^{\beta'} - \rho_l)}{(\Delta H)^{\beta'}\rho_s^{\beta'}}}{\frac{T_m^{\beta}(\rho_s^{\beta} - \rho_l)}{(\Delta H)^{\beta}\rho_s^{\beta}}} \qquad (2)$$

Substituting the experimental values for $T_m^{\beta'}$, $\rho_s^{\beta'}$, ρ_l, $(\Delta H)^{\beta'}$, T_m^{β}, ρ_s^{β}, and $(\Delta H)^{\beta}$ into the above equation, a ratio of gradients of the β' and β forms can be calculated for both PPP and LLL. Our calculations show that in the case of PPP this ratio was 1.20, whereas for LLL it was 1.30. They are greater than 1 and quite similar. This suggests that (i) in a ($T-P$) diagram, an equilibrium straight line of the β' form should be steeper than that corresponding to β and (ii) each of these two equilibrium lines of one substance should be quite similar to its counterpart

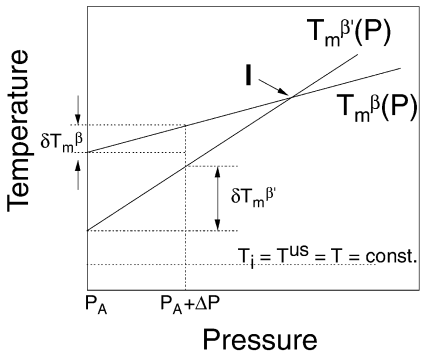

Figure 9. Qualitative pressure−temperature ($P-T$) phase diagram for the β' and β forms of fats. In the isothermal approximation, $T_i = T^{us} = T$ = constant.

of the other substance. Using these two suggestions, we plot the qualitative ($T-P$) phase diagram shown in Figure 9. For the reasons mentioned above, for further discussion, it is reasonable to use this diagram as a common one for both PPP and LLL.

The diagram shown in Figure 9 is in principle measurable, and it should reflect the equilibrium between the solid and liquid phases for both polymorphs over a relatively large range of temperature and pressure. The difference in gradients will result in their intersection at some point defined by a particular pressure and temperature (point I in Figure 9).

4.2. Effects of Pressure and Temperature Change. The sonication of a liquid (melt) is always accompanied by two major simultaneous processes: (a) the periodic change of pressure within a melt induced by the ultrasound wave[20] and (b) the absorption of energy by a melt from the applied ultrasound wave.[21] If the acoustic pressure amplitude is greater than the static (ambient) pressure of a liquid, then process (a) may lead to two concurrent effects: (i) the multiple induction of transient cavitation bubbles[10] and (ii) the violent collapse of the bubbles followed by intense pressure development in their vicinity.[13] Process (b) always results in a temperature increase of a melt.

In the following two sections, a detailed consideration of the impacts of the local change of pressure and temperature on the crystallization of PPP and LLL melts is given.

4.2.1. Effects of Local Changes of Pressure. The amplitudes of sound waves generated by the transducer were above the ambient pressure in the melt (more than 1 bar).[22] Despite the fact that these perturbations produce both fluid flow and pressure waves, it is generally regarded as unlikely that the spatial and temporal scales of the fluid-flow fields would extend down to the level of molecular solid embryos (clusters) relevant to nucleation dynamics.[23] However, it is known that under this condition cavitation, the phenomenon that was observed in our experiments, can be induced.[13] Usually, in a cavitation event a bubble is formed, the radius of which varies between a few tens of micrometers to a few tenths of a micrometer. The bubble overexpands in the negative part of an applied acoustic wave, caves in sharply in the positive half to conceivably 1% of its initial radius, and then rebounds, sending out a pressure pulse.[24−26] The positive pressure developed in this way is remarkably high and localized in space and time.[27−29] Estimated calculations for a moderately supercooled liquid show that at a point approximately 10^{-4} cm from the bubble wall (of diameter $\sim 10^{-5}$ cm) the liquid is subjected to average pressure on the order of 10 kbar over a period of 10^{-9} s.[25] There is no assessment of the magnitude of the negative pressure pulse, but liquids are not known to resist a tensile stress of more than a

few hundred bars.[13] On the other side, thermodynamics implies that at positive pressure pulses of the order of 10 kbar or higher nucleation in supercooled liquids can be induced.[13,27−29] This kind of nucleation is often considered to be a dynamic nucleation[30] because it occurs as a result of the relative motion of the crystallizing liquid. The explanation of this phenomenon is based on the partnership between the classical theory of homogeneous nucleation of a supercooled liquid[31] and the melting-point shift[32] whose magnitude is related to the pressure change via the Clapeyron equation. Here, we consider nucleation rate of the PPP and LLL sonicated melts in the context of recent results[13] obtained by the coupling of the above two approaches.

The rate J at which nuclei are formed is given by[13,31]

$$J = \left(\frac{nkT}{h}\right) \exp\left(-\frac{\Delta G_a}{kT}\right) \exp(-\Delta W) \tag{3}$$

where n is the number of molecules/cm^3, k is the Boltzmann constant, T is the absolute temperature, h is Planck's constant, ΔG_a is the activation energy for a molecule to cross the liquid crystalline interface, and ΔW is the height of the free-energy nucleation barrier for a cluster to overcome before it stands a chance of surviving and growing irreversibly as a crystal. It is given by

$$\Delta W = \frac{16\pi}{3} \frac{\gamma^3}{kT\rho^2(\Delta H)^2\left(\frac{\Delta T}{T_m}\right)^2} \tag{4}$$

in which γ is the free energy of the solid−liquid interface, ΔH is the molar enthalpy of melting, T_m is the melting temperature, ρ is the density of the solid phase, and $\Delta T = T_m - T = T_m - T_i = \Delta T_i$ is the initial supercooling. Each cluster, which can exist for only a very short time, is regarded as having the same relative positions of molecules as it would have in the crystal.

When an ultrasound wave is applied, a sudden onset of crystallization can be induced by high-pressure pulses generated in the vicinity of collapsing cavitation bubbles in an undercooled melt because of the displacement of the melting point.[27] In other words, the pressure rising toward its own peak, in such a small volume of the melt, is accompanied by a local increase in enthalpy, solid−liquid interface energy, density, and melting point. According to ref 13, if ΔP is the difference between the pressure in the vicinity of a collapsing bubble and the ambient (atmospheric) pressure, then the new enthalpy at the new melting point is given by $\Delta H^{us} = \Delta H(1 + \delta)$, where $\delta = \Delta P \Delta V/\Delta H$ in which ΔV is the difference in specific volumes between the undercooled melt and the crystalline phase. Also, $\gamma^{us}/\rho^{us2/3} = (1 + \delta)\gamma/\rho^{2/3}$, where γ^{us} and ρ^{us} are the new solid−liquid interface energy and density, respectively, caused by ultrasonication. Correspondingly, $T_m^{us} = T_m(1 + \delta)$, where T_m^{us} is the displaced melting point. It follows that $\Delta H^{us}/T_m^{us} = \Delta H/T_m$. Therefore, the height of the free-energy nucleation barrier in the vicinity of the collapsing cavity becomes

$$\Delta W^{us} = \frac{16\pi}{3} \frac{\gamma^3(1 + \delta)^3}{kT^{us}\rho^2(\Delta H)^2\left(\frac{\Delta T^{us}}{T_m}\right)^2} \tag{5}$$

where T^{us} is the local change in the temperature of the melt and $\Delta T^{us} = T_m^{us} - T^{us}$ is the corresponding supercooling. Both T^{us} and ΔT^{us} depend on the path taken by the system on the (T−P) plane. In other words, to assess T^{us} and ΔT^{us}, the equation of state of the liquid and the (T−P) diagram are needed. Because we are dealing with the qualitative (T−P) diagram and the equation of state for the two melts is not available, we use the isothermal approximation, which has been proven to be a reasonably good estimate.

For the isothermal process, $T^{us} = T = T_i$. Using the Clapeyron equation and the straight melting lines (Figure 9), we get $\Delta T^{us} = \Delta T_i + \delta T_m$. The first term on the right side is the initial supercooling, and the second one stems from ΔP. Equation 5 changes into

$$\Delta W^{us} = \frac{16\pi}{3} \frac{\gamma^3(1 + \delta)^3}{kT_i\rho^2(\Delta H)^2\left(\frac{\Delta T_i}{T_m} + \delta\right)^2} \tag{6}$$

This expression quantitatively describes the free-energy barrier for nucleation in a very small volume of very high pressure around the collapsing cavity created by applied ultrasound waves. For further discussion, it is suitable to consider a ratio of eq 6 and eq 4. Having taken into account that $\Delta T = \Delta T_i$, we obtain

$$\frac{\Delta W^{us}}{\Delta W} = \left(\frac{\Delta T_i}{T_m}\right)^2 \frac{(1 + \delta)^3}{\left(\frac{\Delta T_i}{T_m} + \delta\right)^2} = \left(\frac{\Delta T_i}{T_m}\right)^2 \frac{\left(1 + \frac{\Delta P \Delta V}{\Delta H}\right)^3}{\left(\frac{\Delta T_i}{T_m} + \frac{\Delta P \Delta V}{\Delta H}\right)^2} \tag{7}$$

This ratio can be estimated for each polymorphic form of PPP and LLL by replacing the corresponding experimental values from Tables 1 and 2 and taking $\Delta P \approx 10$ kbar. A simple calculation shows that $\Delta W^{us}/\Delta W \ll 1$ for either of the two polymorphs for both materials. This implies that the height of the free-energy barrier for nucleation in close proximity to the collapsing cavity is much smaller than the energy barrier in a nonsonicated melt. According to eq 3, a markedly reduced energy barrier around cavitation bubbles can trigger nucleation prematurely in one or more spots, resulting in an increase in the nucleation rate J. Because the nucleation rate is inversely proportional to the induction time,[33] $J \propto 1/\tau$, an elevated nucleation rate due to the application of sonication will lead to decreasing induction times. A striking decrease of the induction times obtained under the sonication of both PPP and LLL supercooled melts with respect to those without sonication (Table 2) shows very close agreement with the proposed model. However, the model does not explain why under certain conditions (sections 3.2 and 3.4.1) only the β form was nucleated whereas at lower crystallization temperatures both forms appeared (section 3.4.2). This inadequacy indicates that cavitation is a necessary but not sufficient condition for dynamic nucleation; additional factors need to be taken into account.

We argue that additional factors such as the duration of the final stages of collapsing cavities and the lifetimes of subcritical nuclei and their stability may play critical roles in the nucleation of a particular polymorph. In a moderately supercooled melt similar to those used in our experiments, the duration of the final stage of a collapsing bubble, at which the high-pressure pulse is developed in its vicinity, is on the order of nanoseconds.[10,29] To generate nuclei of a particular polymorph, this duration should be on the order of or longer than the lifetime of a cluster (subcritical nuclei). At this stage, we hypothesize that because the β' form is less stable than the β form the lifetime scales of β' clusters at the initial crystallization temperatures of $T_i = 50$ °C for PPP and $T_i = 30$ °C for LLL are probably too short compared to the duration of the collapsing cavities. Therefore, β' clusters were dissolving before producing any

continuing effect. On the contrary, the more-stable β clusters, which were subjected to the same local high pressure but with a lifetime comparable to the duration of the final stage of the collapsing bubble, would suddenly achieve the size of critical nuclei, and irreversible precipitation of this form would begin. Following the same philosophy, it appears that the observed precipitation of both forms in the LLL melt (section 3.4.2) was brought about by an increased lifetime of both the β' and β clusters because of the lower crystallization temperature, T_i = 25 °C, at which the sonication was applied.

Finally, locally induced ΔP should also influence ΔG_a by an increase in the viscosity of the supercooled melt. For simple systems with small molecules, this effect should be negligible, whereas for relatively large molecules, an increase in the viscosity could substantially slow the nucleation rate.[34] The markedly reduced induction times for both PPP and LLL melts due to sonication suggest that ΔG_a has not been appreciably influenced by ΔP.

4.2.2. Effect of Temperature Change. The observed post-sonication increase of the crystallization temperature in both the PPP and LLL melts of approximately 2.5 °C could be interpreted as the result of the overall heat generated by (1) the dissipation of acoustic energy and (2) heat formation in the highly compressed gas in the cavitation bubbles.

Contribution 1 arises from sources inherent in a liquid (viscous losses, heat-conduction losses, and losses related to internal molecular processes) and sources associated with the boundaries of the liquid.[35]

Contribution 2 has been conclusively confirmed by recent experiments on the sonoluminescence by single compressed cavitation bubbles,[36,37] which have shown an astonishingly short duration (<50 ps) of the flashes of light emitted by single cavitation bubbles. An earlier estimate based on the sonoluminescence spectra analysis[38,39] suggests that temperatures of the order of 10^4 K can occur within the bubble. It has also been shown that all of the energy transferred from a spherical source of radius 5×10^{-4} cm (an average radius of the bubble during the period of high temperature), in terms of radiation and conduction, is absorbed by a thin shell of liquid between the wall and an outer radius of 6×10^{-4} cm. This would lead to an average temperature increase of a few degrees. However, the actual effect of the heat at a point 10^{-4} cm from the wall of the bubble was negligible,[27] resulting in no interference with stimulated nucleation in the vicinity of the collapsing cavities. Despite the fact that these experiments have been done on the collapsing cavities of supercooled water, it seems reasonable to suppose that the heat generated in the compressed bubbles in PPP and LLL will follow similar pathways. This belief is based on the strikingly reduced induction times in the presence of sonication (Table 2). Having taken into account (a) that sonication was applied once a desired crystallization temperature was achieved and (b) the model that we have adopted in this discussion, the induction times for nucleation in both melts should be virtually zero. The fact that the observed induction times were a few tens of seconds does not imply that any of these times are real induction times because at present there is no available experimental technique, including SAXS, by which the onset of nucleation events can be detected. As mentioned earlier (section 3.1), the first diffraction signal in the SAXS spectra corresponds not to nucleation itself but to an appreciable amount of diffracting material that has grown in the system since the nucleation has occurred. Apart from this, the observed induction times were influenced to some extent by the decelerated growth of the prediffracting material due to the post-sonication continuation of the temperature increase of the crystallizing melt. It is quite likely that this temperature increase (first increase on the $T(t)$ diagrams) is the consequence of a time-dependent heat transfer from the "hot" spots created by the collapsing cavities toward the bulk of the melt.

The above discussion allows us to conclude that the nucleation processes in PPP and LLL occurred simultaneously with applied ultrasound. The observed temperature increase during and after the application of ultrasound results from the ultimate conversion of contributions 1 and 2 into an increase of the random thermal energy of the system as a whole. This energy (heat), apart from the decelerating growth of the already nucleated melt, should not have any significant effect on the nucleation itself because the process of heat transfer from the hot spots into the bulk of the melt is probably much slower than a successful nucleation process in the high-pressure vicinity of the collapsing bubbles.

Conclusions

The present investigation has been aimed at the effects and mechanisms of ultrasound-induced crystallization in PPP and LLL supercooled melts. Using in situ time-resolved SAXS/WAXS techniques and existing knowledge on the dynamic nucleation of collapsing cavities, it was possible to describe, for the first time, the behavior of the most important parameters and the events that characterize the crystallization of these systems. Our results can be summarized as follows. (1) A dramatic shortening of the induction times (an increase in the corresponding nucleation rates) observed in the sonicated melts was caused by two major factors: (a) the ultrasound-stimulated nucleation occurred in the high-pressure vicinity of the collapsing bubbles because of the melting-point shift and the consequent increase in supercooling and (b) a remarkable decrease of the free-energy barrier for nucleation compared to that without sonication. (2) It was shown that the interplay of sonication and the temperature of supercooled melts is crucial for obtaining only the β polymorph. (3) The observed increase in the temperature of the melt during and after sonication, before the induction time was detectable, was explained by the overall absorption of ultrasound energy. The post-sonication increase in the temperature of a melt was due to heat transfer from the hot spots to the volume of the melt. This heat should not have any significant effect on the nucleation of either of the two polymorphs.

Apart from the above findings, these studies clearly indicate the main research avenues to be followed. To improve our knowledge and predictability in terms of desired polymorphism, induction times, and nucleation rates, a better understanding of the following issues is crucial: (i) ($T-P$) phase diagram for the β' and β forms, (ii) stability (lifetime) of different polymorphic forms as a function of supercooling temperature, (iii) mechanism and lifetime of collapsing cavities, and (iv) basic mechanism of the dynamic nucleation in the vicinity of a collapsing bubble. In addition, knowledge of an equation of state for the studied materials may be of great use, in particular, when a comprehensive test of the most adequate thermodynamic conditions, at which dynamic nucleation occurs, needs to be established.

Acknowledgment. We gratefully acknowledge the financial support of this work by the Venture Business Laboratory (VBL) of Hiroshima University, Japan, and the U.K. EPSRC through grant GR/M73637. We acknowledge the support of the director and staff of the Daresbury Laboratory through the provision of facilities for SAXS/WAXS experiments.

References and Notes

(1) *Advances in Crystal Growth Research*; Sato, K., Furukawa, Y., Nakajima, K., Eds.; Elsevier Science B. V.: Amsterdam, 2001; Part 3, pp 351−419.

(2) *Lipid Technologies and Applications*; Gunstone, F. D., Padley, F. B., Eds.; Marcel Dekker: New York, 1997; Part 2, pp 113−263.

(3) *Bailey's Industrial Oil and Fat Products*, 5th ed.; Hui, Y., Ed.; Wiley-Interscience: New York, 1996; Vol. 3.

(4) Formo, M. W. In *Bailey's Industrial Oil and Fat Products*, 4th ed.; Swern, D., Ed.; Wiley & Sons: New York, 1979; Vol. 1, pp 177−232.

(5) Sato, K. *Chem. Eng. Sci.* **2001**, *56/57*, 2255−2265.

(6) Mason, T. J.; Paniwnyk, L.; Lorimer, J. P. *Ultrason. Sonochem.* **1996**, *3*, S253−S260.

(7) Mason, T. J. In *Ultrasound in Food Processing*; Povey, M. J. W., Mason, T. J., Eds.; Blackie Academic & Professional: London, 1998; pp 105−126.

(8) Hem, S. L. *Ultrasonics* **1967**, *5*, 202−207.

(9) Enomoto, T.; Sung, T. H.; Nakagawa, Z. E.; Lee, S. C. *J. Mater. Sci.* **1992**, *27*, 5239−5243.

(10) Ohsaka, K.; Trinh, E. H. *Appl. Phys. Lett.* **1998**, *73*, 129−131.

(11) Baxter, J. F.; Moris, G. H.; Gaim-Marsoner, G. European Patent Application 95306833.5, 1995.

(12) Higaki, K.; Ueno, S.; Koyano, T.; Sato, K. *J. Am. Oil Chem. Soc.* **2001**, *78*, 513−518.

(13) Lee, C. P.; Wang, T. G. *J. Appl. Phys.* **1992**, *71*, 5721−5723.

(14) Small, D. M. In *The Physical Chemistry of Lipids*, 2nd ed.; Plenum Press: New York, 1988; pp 97−101, 123−125, 347−352.

(15) Brass, W.; Derbyshire, G. E.; Ryan, A. J.; Mant, G. R.; Felton, A.; Lewis, R. A.; Hall, C. J.; Greaves, G. N. *Nucl. Instrum. Methods Phys. Res., Sect. A* **1993**, *326*, 587−591.

(16) In ref 14, pp 368−369.

(17) Sato, K.; Goto, M.; Yano, J.; Honda, K.; Kodali, D. R.; Small, D. M. *J. Lipid Res.* **2001**, *42*, 338−345.

(18) Van Langevelde, A.; van Malseen, K.; Driessen, R.; Goubitz, K.; Hollander, F.; Peschar, R.; Zwart, P.; Schenk, H. *Acta Crystallogr., Sect. B* **2000**, *56*, 1103−1111.

(19) Jensen, L. H.; Mabis, A. J. *Acta Crystallogr.* **1966**, *21*, 770−781.

(20) Wu, C. C.; Roberts, P. H. *Phys. Rev. Lett.* **1992**, *70*, 3424−3427.

(21) Mason, W. P. *Physical Acoustics*; Academic Press: New York, 1965; Vol. 2A.

(22) Leighton, T. G. *The Acoustic Bubble*; Academic Press: New York, 1997.

(23) Kurz, W.; Fisher, D. J. *Fundamentals of Solidification*; Trans Tech Publications: Switzerland, 1984; p 184.

(24) Apfel, R. E. *J. Acoust. Soc. Am.* **1981**, *69*, 1624−1633.

(25) Prosperetti, A. In *Frontiers in Physical Acoustics*; Sette, D., Ed; North-Holland: New York, 1986.

(26) Hickling, R.; Plesset, M. S. *Phys. Fluids* **1964**, *7*, 7−14.

(27) Hickling, R. *Nature (London)* **1965**, *206*, 915−917.

(28) Hickling, R. *Nature (London)* **1965**, *207*, 742.

(29) Hickling, R. *Phys. Rev. Lett.* **1994**, *73*, 2853−2856.

(30) Chalmers, B. *Principles of Solidification*; R. E. Krieger Publishing Co.: Malabar, FL, 1982; p 86.

(31) Turnbull, D.; Fisher, J. C. *J. Chem. Phys.* **1949**, *17*, 71−73.

(32) Chalmers, B. In *Liquids: Structures, Properties, Solid Interactions*; Hughel, T. J., Ed.; Elsevier: New York, 1965; p 308.

(33) Mullin, J. W. *Crystallization*, 4th ed.; Butterworth-Heinemann: Oxford, U.K., 2001.

(34) Bridgman, B. W. *The Physics of High Pressure*; Macmillan: New York, 1971.

(35) Kinsler, L. E.; Frey, A. R.; Coppens, A. B.; Sanders, J. V. *Fundamentals of Acoustics*, 4th ed.; Wiley & Sons: New York, 2000.

(36) Barber, B. P.; Patterman, S. J. *Nature (London)* **1991**, *352*, 318−320.

(37) Barber, B. P.; Hiller, R.; Arisaka, K.; Fetterman, H.; Patterman, S. J. *J. Acoust. Soc. Am.* **1992**, *91*, 3061.

(38) Hickling, R. *J. Acoust. Soc. Am.* **1963**, *35*, 967−974.

(39) Finch, R. D. *Ultrasonics* **1963**, *1*, *87*.